Optical Properties of Modulation-Doped Quantum Wells

1987 Phys. Scr. 1987 129

(http://iopscience.iop.org/1402-4896/1987/T19A/019)

Physica Scripta. Vol. T19, 129–135, 1987.

Optical Properties of Modulation-Doped Quantum Wells

C. Delalande

Groupe de Physique des Solides de l'Ecole Normale Supérieure, 24 rue Lhomond, F-75005 Paris, France

Received April 7, accepted April 22, 1987

Abstract

The optical properties of one-side modulation-doped quantum wells are described and compared with theory in the Hartree approximation. The electron areal density is modified by voltage application or illumination and a measurement of the Band Gap Renormalization is obtained. The role of excited states, when populated, is emphasized.

1. Introduction

Transport properties of modulation-doped heterojunctions and optical properties of nominally undoped quantum wells (QW's) are the subjects of an abundant literature, especially in the GaAs/Ga(Al)As system. Unfortunately, except for the Raman effect [1] the single heterostructures do not allow optical studies as the built-in electric field prevents the photocreated hole (electron) to recombine with an electron (hole) of the Fermi sea. The poor quality of the inverted interface [2], i.e., GaAs grown on top of Ga(Al)As, induces a rather low mobility in symmetrically doped QW's and smooth features in optical spectra [3]. The growth of one-side modulation-doped (MD) QW's leads to an important improvement of the mobility of the carriers [4], owing to the larger spatial separation achieved between the quasi-bidimensional (2D) electron gas and the inverted interface and to the absence of deleterious Si segregation or in-well diffusion which apparently takes place when one attempts to dope the inverted interface.

One of the fundamental interests of these structures is the study of many-body effects in a quasi-2D electron gas. A great amount of work has been done in the 3D case either in metals or in electron-hole plasmas photocreated in semiconductors [5]. It is also possible to create in an undoped QW by optical absorption in the high excitation regime a two-component plasma [6] whose temperature and concentration can be deduced from lineshape analysis [7]. MDQW's offer a unique system of a 2D one-type carrier plasma which can be studied at low temperature (2 K) by photoluminescence and photoluminescence excitation spectroscopy [3, 8]. The electron density n_s can be determined in these structures independently of the optical data, by Shubnikov–de-Haas measurements performed under the same illumination conditions. Moreover, n_s can be varied either by applying a weak in-plane electric field [9], or by illuminating the sample by photons of energy larger than the Ga(Al)As barrier gap [9, 10], or by applying an electric field parallel to the growth axis through a semi-transparent Schottky contact. A low-temperature one-component plasma of variable density in a QW of given thickness can thus be studied. The experimental results are described in the first section of this paper.

Before obtaining quantitative informations on many-body properties, a calculation of the energy levels in the growth direction and of the in-phase dispersion relations in the Hartree approximation is necessary. This calculation must take into account the band-bending induced by the presence of the electron gas in the QW. The complex structure of the valence-band dispersion relations which results from the coupling between various subbands at non-vanishing in-plane wavevector $\boldsymbol{k}_\perp$ cannot be ignored. The assumptions and the results of a theoretical calculation which uses a self-consistent Hartree approximation and the Luttinger Hamiltonian for the valence-band are recalled in the second section. It is worth noticing that the results are checked both by the assignment of high-energy transitions as well as extrapolation at vanishing n_s where the many-body problem becomes the excitonic effect, which is now well known in QW's.

By a comparison between experimental and theoretical results, the main optical properties of MDQW's are evidenced. (i) A Stokes shift between the excitation onset and the photoluminescence peak appears. This Stokes shift, the Moss-Burnstein shift, is proportional to n_s and is due to the Pauli principle. (ii) Owing to screening and occupancy effects, the exciton has no more bound state. Excitation and luminescence involve band-to-band processes at $\boldsymbol{k}_\perp = \boldsymbol{k}_F$, the Fermi wavevector, and $K = 0$ respectively. (iii) An apparent shrinkage of the band-gap which compensates partly the size-confinement effects is observed. One part of this shrinkage is due to the curvature of the bottom of the well. But a careful comparison with the Hartree calculation, which takes into account this band-bending effect, allows the measurement of the density dependence of the decrease of the band-gap due to exchange and correlation mechanisms, the band-gap renormalization (BGR), in quasi-2D systems. A comparison with available theoretical data will be given.

Finally, in a wider MDQW containing a larger concentration of carriers, two conduction subbands can be populated. Because of the band-bending, it is shown both experimentally and theoretically that the larger overlap between the excited conduction subband and the fundamental hole levels promotes a luminescence involving the excited subband.

2. Experimental results

The samples whose study is reported here have been grown by molecular beam epitaxy. They present nominal carrier densities n_s in the 10^{11} to $10^{12}\,cm^{-2}$ range and low temperature mobilities as high as $290\,000\,cm^2/Vs$ (Table I). The actual thickness is estimated, when possible, by measurement of the photoluminescence and excitation peak energies in the limit $n_s \to 0$ and taking into account the excitonic effect. The growth sequence is shown in the upper part of Fig. 1. The

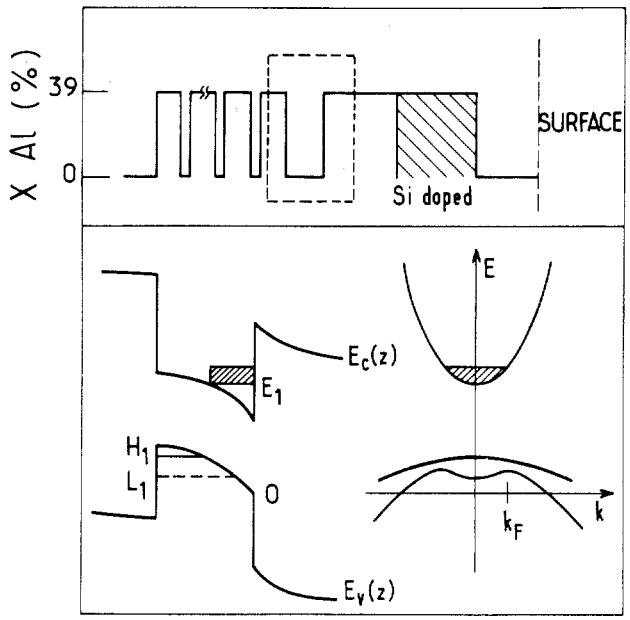

Fig. 1. Upper part: schematic aluminum profile of the samples under consideration. Lower part: (left) band edges in the growth direction and (right) in-plane dispersion relations of the MDQW.

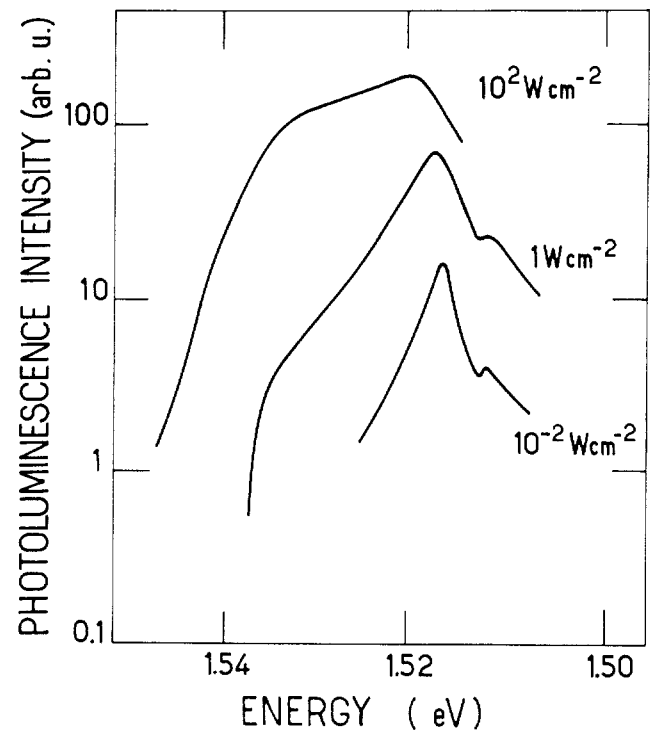

Fig. 2. Photoluminescence of the 150 Å thick, $4.5 \times 10^{11}\,cm^{-2}$–$n_s$ 1413 MDQW at three excitation powers.

aluminium concentration of the barrier is 0.38. A GaAs/$Ga_{0.62}Al_{0.38}As$ superlattice (typically 7×35 Å + 8×100 Å) was grown before the QW under consideration in order to improve the quality of the inverted interface. The Si concentration in the doped $Ga_{0.62}Al_{0.38}As$ layer is in the $10^{18}\,cm^{-3}$ range. A 250 Å-thick GaAs cap layer was grown on top of the overall structure. Rather crude processes have been carried out to determine the carrier density (two Ge-Au diffusions separated by 4 mm, contacting the 2D gas) and to apply to the QW a variable electric field perpendicular to the 2D plane (100 Å-thick semi-transport Cr Schottky contact evaporated onto a $2 \times 2\,mm^2$ spot of the sample). It is worth noticing that the electron concentration must be determined – when possible – under the same illumination conditions as the optical measurements i.e., in the same cryostat. The increase of n_s induced by a permanent photoconductivity effect is illustrated in Table I. The same n_s values have been found theoretically [11] by adapting to our heterostructures Stern's approach [12]. At low temperature and under illumination the Fermi level is assumed to be in the conduction-band of the doped part of the Ga(Al)As layer and not on the donor level.

All the experiments reported here have been performed at 2 K in pumped-liquid He cryostats. The photoluminescence of the 150 Å-thick 1413 sample ($n_s = 4.5 \times 10^{11}\,cm^{-2}$) when excited by 1.55 eV light is shown in Fig. 2. The structure appearing on the low-energy side can be proved, using excitation spectroscopy, to originate from the GaAs buffer layer. The main peak contains both the buffer and quantum well luminescences, the low-energy side being essentially due to the buffer and the high-energy side to the QW (for lower n_s values, these two contributions are clearly resolved). The precise location of the QW luminescence has been obtained by extrapolating magneto-luminescence experiments, where the buffer and QW luminescences are resolved [13]. When the power of the incident light is increased over 4 orders of magnitude, the peak is slightly blue-shifted (~3 meV). A high-energy tail develops and a shoulder appears on this high-energy tail, approximately 13 meV above the energy of the luminescence peak. This shoulder can be assigned to a transition involving a light-hole level, which becomes populated at high excitation.

The photoluminescence excitation spectra have been carried out by tuning a LD700 cw dye laser. Figure 3 shows the excitation spectrum of the 130 Å-thick, $2.9 \times 10^{11}\,cm^{-2}$-$n_s$ 1604 sample as well as the luminescence spectrum (dashed line). Two characteristic features must be emphasized: the rather large broadness of the first two excitation peaks as compared to high quality undoped QW's, and the 13 meV Stokes shift between the first excitation peak and the photoluminescence line. The first feature is related to the dis-

Table I.

Sample number	Nominal thickness (Å)	Estimated thickness (Å)	n_s dark ($10^{11}\,cm^{-2}$)	n_s illumination ($10^{11}\,cm^{-2}$)	Mobility ($10^5\,cm^2/Vs$)
1383	325	–	6.6 (77 K)	10 (2 K)	1.1 (77 K)
1413	150	150	2.3 (10 K)	4.5 (2 K)	2 (10 K)
1543	160	–	3.55 (10 K)	–	2.9 (10 K)
1604	150	130	Freeze out (77 K) 0.5 (300 K)	2.9 (2 K)	–

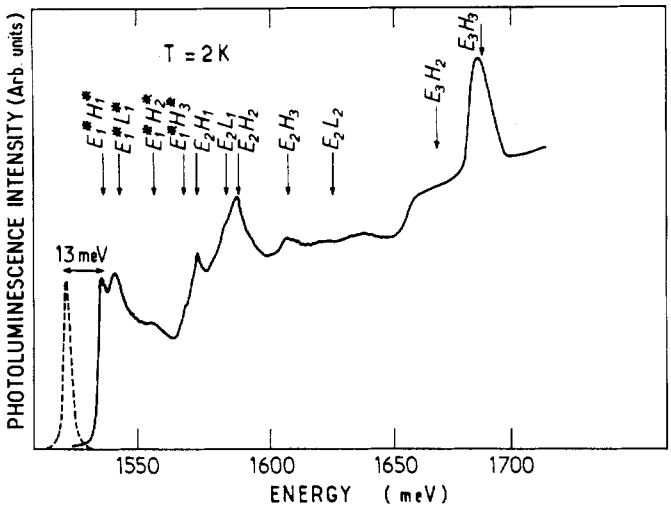

Fig. 3. Low temperature photoluminescence (dashed line) and photoluminescence excitation spectrum of the 130 Å thick 2.9 $10^{11}\,cm^{-2}$–n_s 1604 MDQW. The arrows indicate the energies of the transitions calculated in the Hartree approximation and reduced by a Band Gap Renormalization of 19 meV. The transitions without asterisks occur at $k_\perp = 0$, the ones with asteriks at $k_\perp = k_F$.

appearance of the excitonic effect: the structures seen in the excitation spectra will be identified with subband-to-subband transitions. The second feature is due to the Moss–Burnstein shift: owing to the Pauli principle, the onset of the excitation of the E_1-HH_1 transition occurs at $k_\perp = k_F = \sqrt{2\pi n_s}$, the Fermi wavevector [3], whereas the luminescence occurs at $K = 0$ after relaxation of the photoexcited holes. Taking for the in-plane carrier masses $m_e = 0.07m_0$ and $m_{hh} = 0.2m_0$, which is consistent with the following calculations of the valence-subband dispersion relations, this Stokes shift can be calculated to be $E_F(1 + m_e/m_{hh}) = 13.4$ meV for $n_s = 2.9 \times 10^{11}\,cm^{-2}$. Whenever optical experiments and Shubnikov–de-Haas measurements have been carried out in the same experimental set-up on various samples, such an agreement has been found. This shows that, conversely, a value of n_s can be found from the Stokes shift value, when this comparison can not be carried out, owing to the experimental set-up or to heating or inhomogeneity problems.

This Stokes shift, and consequently n_s, has been varied from its nominal value in three ways. Following Chaves *et al.* [10], an intense illumination by an Argon laser (the effect does not occur when the intense beam has an energy lower than the Ga(Al)As band-gap) provides an increase of the luminescence energy. By performing simultaneously excitation spectroscopy with a weak chopped dye laser, Delalande *et al.*

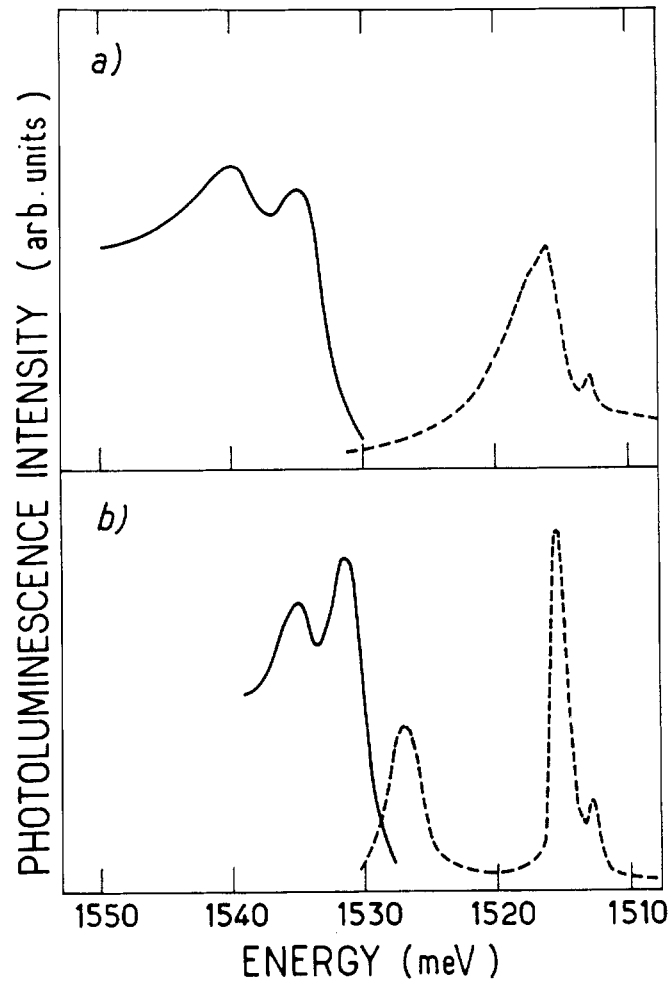

Fig. 4. Photoluminescence (dashed lines) and photoluminescence excitation spectrum (full line) of the 1413 MDQW (lower part) obtained with a 30 mW/cm² LD700 dye laser, (a) without illumination by an Argon laser, (b) under an illumination of the order of 3 W/cm². The low energy part (a) and the low energy line (b) of the photoluminescence involve the buffer GaAs layer.

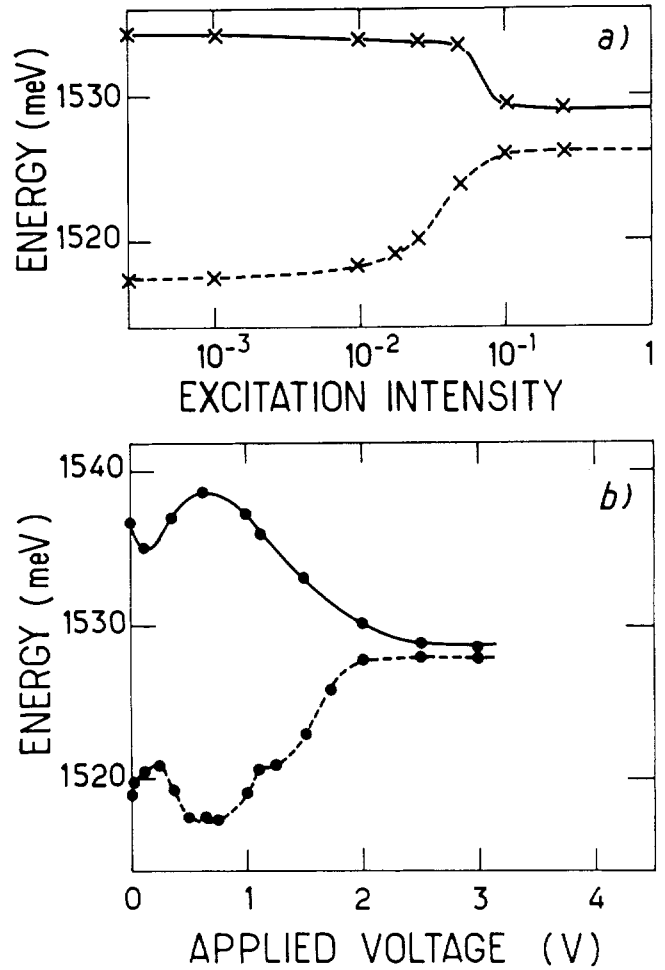

Fig. 5. Energy of the luminescence peak (dashed lines) and of the first excitation peak (full lines) as a function (a) of the intensity of the Argon laser illumination, (b) of the applied in-plane voltage. In case (a) the full scale intensity is of the order of 30 W/cm². In case (b), the length of the Hall bridge is 3 mm.

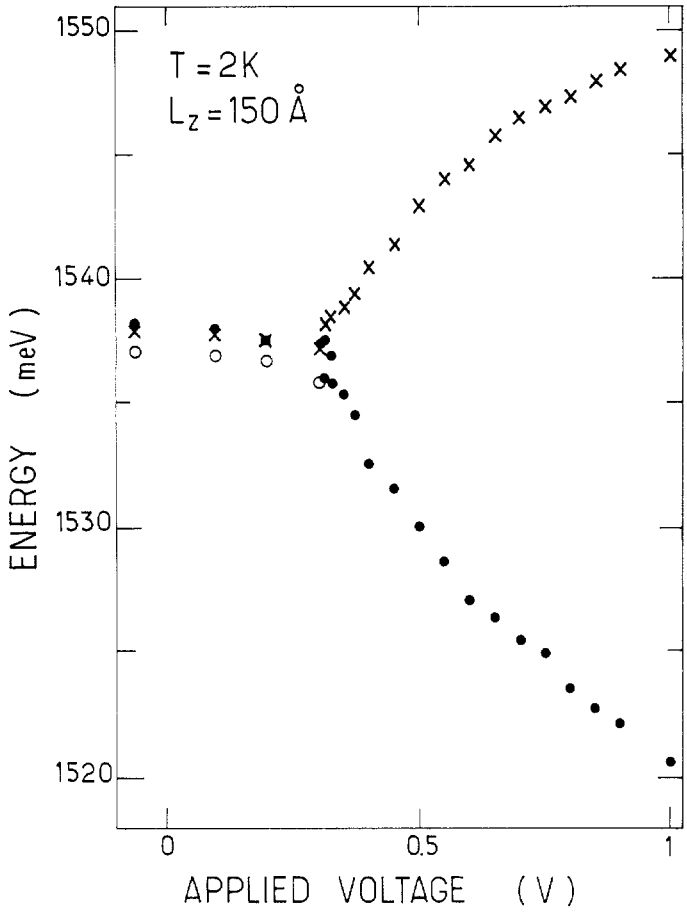

Fig. 6. Photoluminescence peak energy (full dots) and first excitation peak energy (crosses) of the 1604 MDQW as a function of the Schottky voltage V. The circles refer to the secondary luminescence peak accounted for well width fluctuations (see Fig. 7).

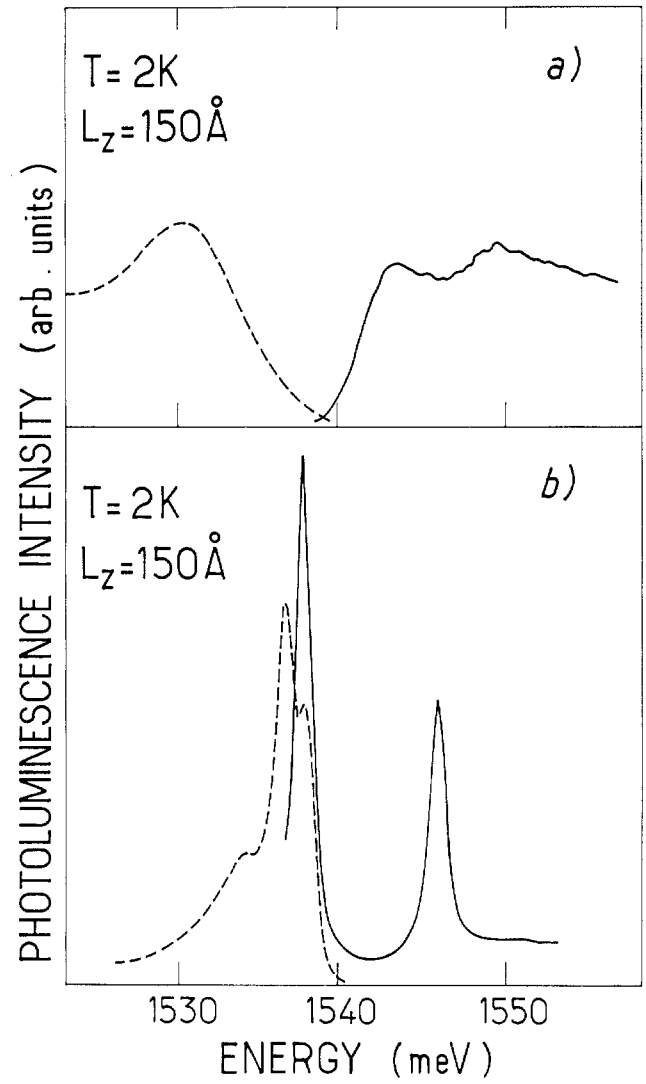

Fig. 7. Photoluminescence (dashed line) and excitation (full line) of the 1604 sample with a Schottky voltage (a) $V_s = +0.5$ V; (b) $V_s = -2$ V.

[9] have found a simultaneous decrease of the excitation onset energy, and thus of n_s (Fig. 4). It has been proposed that the holes photocreated in the Ga(Al)As barrier move into the MDQW and recombine there with the electrons of the Fermi sea, inducing a decrease of n_s in the MDQW. The steady state is controlled by tunnelling of electrons from the doped part of Ga(Al)As towards the QW.

It is also possible to control n_s by applying a steady and weak in-plane electric field. A 3 mm-length and 300 μm-width Hall bridge has been processed for this purpose. Here also, the electronic structure is tested by 2 K luminescence and excitation spectroscopy in the center of the structure. The behaviour is the same as previously. Although the physical process responsible for the decrease of n_s with the applied voltage (or the current which is of the order of 5 mA for an in-plane voltage of 3 V) is not understood, it is found that at 10 V/cm, the Stokes shift is reduced to 1 meV (Fig. 5), with no dramatic heating of the electron gas, in contrast with other reports [14], but with a narrowing of the lines.

Finally, like in an usual FET transistor, n_s can be varied by applying a voltage between the electron gas and a semi-transparent Schottky contact evaporated on the surface. This experiment has been performed in the 1604 sample. The pseudo flat-band condition, in which the behaviour is found to be the same as without Schottky contact, occurs for $V_{\text{Schottky}} - V_{\text{2DGas}} = 0.5$ V. When V_{Schottky} is increased, the energy corresponding to the onset of the excitation increases while the luminescence peak energy decreases, with a value of the Stokes shift corresponding to $n_s = 7 \times 10^{11}$ cm^{-2}. We found below 0.3 V a zero Stokes shift (Fig. 6). Note also the striking evidence of the narrowing of the excitation and luminescence peaks, which evidences a recovery of the excitonic behaviour characteristic of undoped QW's (Fig. 7). The doublet which appears in the luminescence spectrum can be attributed to well-width fluctuations [15].

3. Energy levels in the Hartree approximation and assignment of the lines

The energy levels, and firstly the conduction levels, have been calculated within the Hartree approximation. For the thin enough wells, all the electrons are found in the lowest conduction subband E_1 at low temperature. The condition-band dispersion can be considered as parabolic in GaAs (mass $m_e = 0.07m_0$) and the wave functions $\chi_n(z)$ are solutions of the coupled Schrödinger and Poisson equations:

$$[P^2/2m_e + V_B Y(z)Y(L - z) - e\varphi_{sc}(z)]\chi_n(z) = \varepsilon_n\chi_n(z) \quad (1)$$

$$d^2\varphi_{sc}(z)/dz^2 = 4\pi e/\kappa[n_s\chi_1^2(z) + N_A^-(z)] \quad (2)$$

where $V_B = 1.247 \times 0.6x$ is the $Ga_{1-x}Al_xAs$ conduction-band offset [16], Y is the step function, $\kappa = 12.4$ the dielectric constant and $N_A^-(z)$ the residual p-type doping in the nomi-

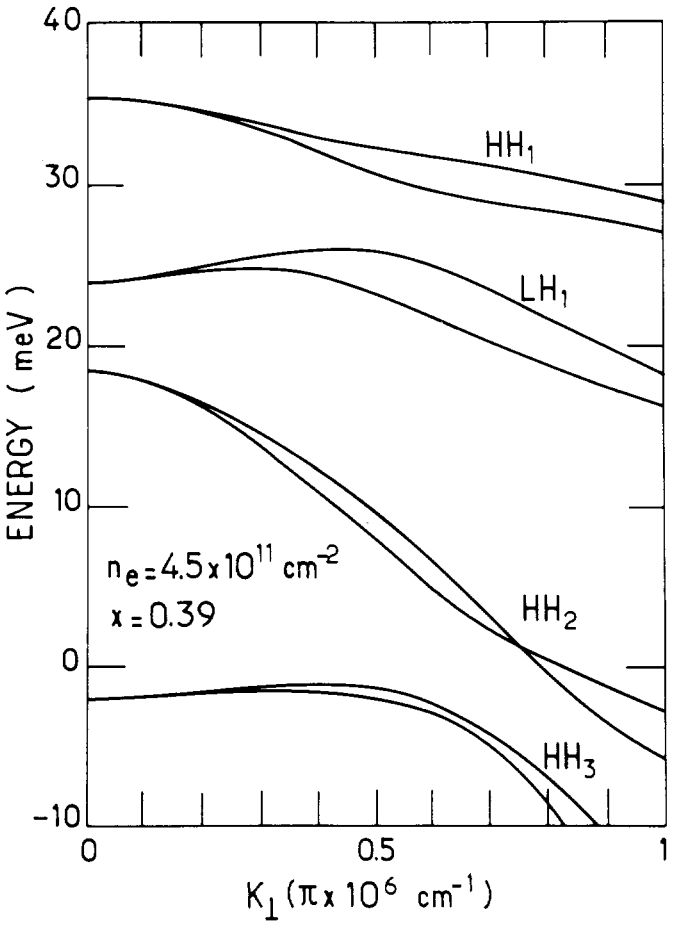

Fig. 8. $n_s = 4.5 \times 10^{11}$ 1413 sample in-plane dispersion relations of the valence band.

nally undoped layer. The z origin is taken at the interface of the doped side and L is the well thickness. n_s is known in the above equations, i.e., the thermodynamic equilibrium throughout the structure is supposed to be solved and has been already determined independently [11]. The coupled equations (1) and (2) are solved by a variational method.

$$\chi_1(z) = N \exp(-\beta z)\chi_1^{(0)}(z) \tag{3}$$

where β is the variational parameter and $\chi_1^{(0)}(z)$ the ground state wave function of the quantum well under flat-band conditions. This method [17] compares favorably with more elaborate schemes [18, 19]. For $n_s = 4.5 \times 10^{11}\,\mathrm{cm}^{-2}$, $L = 150$ Å and $N_A^- = 10^{14}\,\mathrm{cm}^{-3}$, the potential energy difference across the well is calculated to be 47 meV and the confinement energy ε_1 is 52 meV.

Once $\varphi_{sc}(z)$ is determined, the excited electronic levels ε_i ($i > 1$) are numerically calculated. With the use of the Luttinger Hamiltonian for the valence-band, the in-plane dispersion relations of the valence subbands are also determined following the treatments of Altarelli [20] and Ando [21]. The set $\chi_n^{(0)}(z)$ of the wavefunctions of the QW under flat band conditions is taken as troncated basis for this determination (conduction wavefunctions for the determination of ε_i, heavy hole and light hole wavefunctions for the determination of the valence-subband dispersion). A determination of the self-consistent potential has also been carried out by this numerical method and provides the same results as the variational method within a couple of meV's.

A calculated in-plane dispersion relation of the valence-band is presented in Fig. 8. The most striking feature is the large mixing between various hole subbands. In particular, the energy difference between the fundamental heavy-hole HH_1 and light-hole LH_1 levels is significantly smaller at the Fermi wavevector, near $k_\perp = 0.5$ in the units of Fig. 8, than at $k_\perp = 0$. One notices also the strong upward shift of the hole levels due to the tilted aspect of the QW band-edge profile. The lack of inversion symmetry also lifts the Kramer degeneracy (this lifting is not resolved in the optical experiments and the mean value of Kramer's doublets are taken for comparison with experiment), and lifts the Δn even selection rule in intersubband optical transitions.

The structures observed in the luminescence excitation spectra have been identified with vertical subband-to subband optical transitions ($k_\perp^{\text{initial}} = k_\perp^{\text{final}}$). The transitions ending at E_1 are considered to take place at $k_\perp > k_F$, because of the Pauli principle. The fact that peaks and not steplike structures are observed may arise from enhanced absorptions due to unbound excitons [22–24] and/or from resonances in the relaxation mechanisms. With these assumptions, the existence and energy position of the observed transitions (arrows in Fig. 3) and in particular the energy difference between HH_1 and LH_1 at $k_\perp = k_F$, are well reproduced by the calculations. This provides evidence of the positive curvature of the LH_1 subband in the vicinity of $k_\perp = 0$. Also in agreement with experiment is the calculated Stokes shift between the transition E_1–HH_1 at $k_\perp = k_F$ (excitation and $k_\perp = 0$ (luminescence). But to obtain a good agreement between the absolute positions of the calculated and observed transitions, it is necessary to use a GaAs band-gap which is 19 meV smaller than the GaAs one. The apparent shrinkage of the gap induced by band-bending in the Hartree approximation is not sufficient, one needs a many-body approach.

4. Band gap renormalization

Many-body effects in 2D or quasi 2D systems were recently evaluated in a series of papers [25–28] following various approximations. A discussion of these approximations is outside the scope of this paper. Unfortunately, the calculations are generally not performed in our peculiar geometry, i.e., one-side MDQW's of a given thickness, and only a rough comparison with available theories is possible. The qualitative behaviour can be summarized as follows. With increasing doping concentration, many-body interactions lead to a renormalization of the single-particle states and of the electron-hole interaction and to a blocking of the available phase space as a result of the Pauli principle. Exchange and correlation effects lead to a red shift of the band-gap and, at low doping concentration, to a lowering of the exciton binding energy. When the doping concentration exceeds a critical value, the renormalized band-gap falls below the exciton level so that excitonic bound states are no longer stable. Excitation and luminescence involve then band-to-band processes with some resonances which are due to final state interactions, and many-body effects can be regarded as a rigid shift of the electron and hole bands towards each other (the Band Gap Renormalization BGR).

Figure 7 has given a dramatic evidence of the weakening of the electron–hole resonances when the carrier density is increased and, conversely, of the strong excitonic behaviour when $n_s \to 0$. The critical density where the bound state of

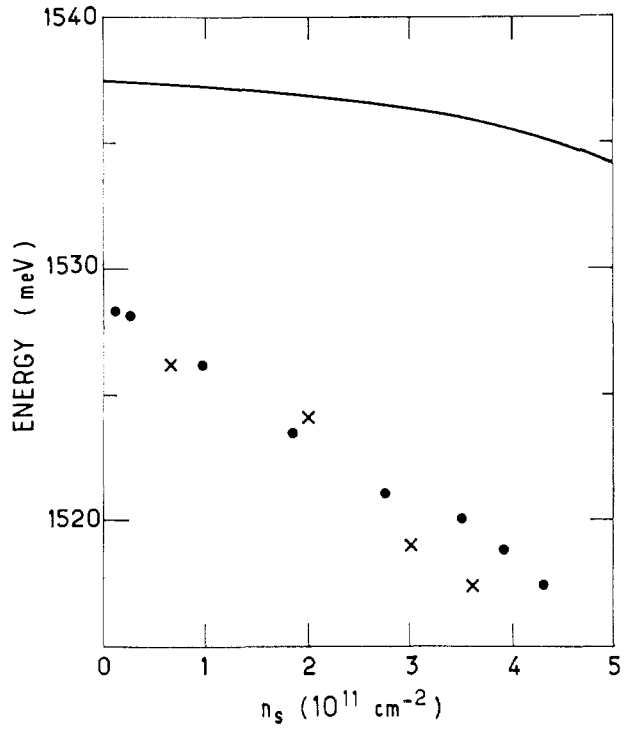

Fig. 9. 150 Å-thick 1413 sample line: n_s dependence of the band-to-band transition energy calculated in the Hartree approximation as described in the text. Crosses: experimental data obtained by in-plane voltage control. Dots: data obtained by Argon laser illumination.

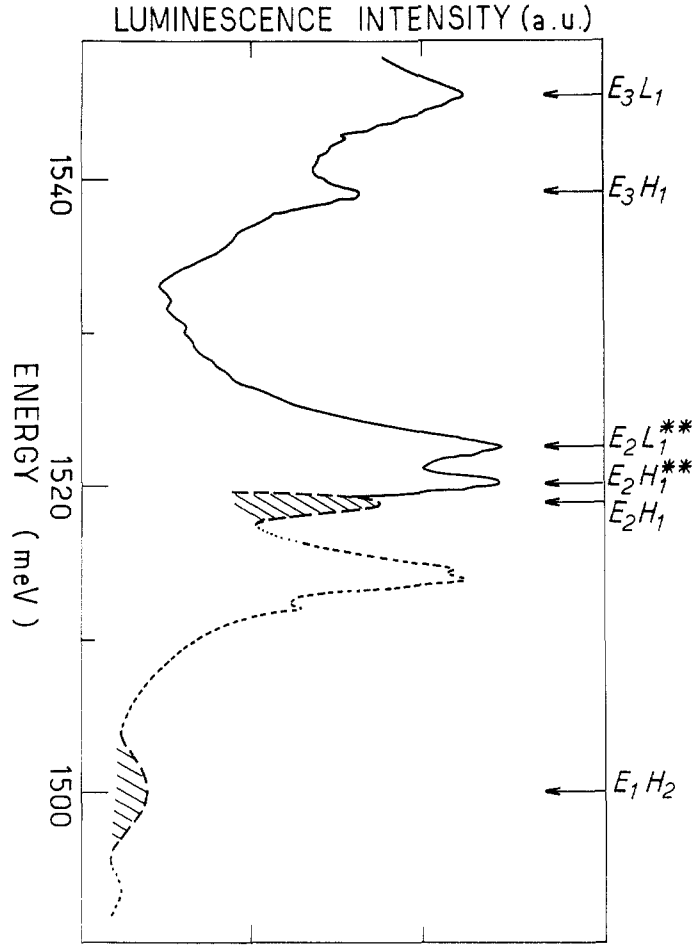

Fig. 10. Photoluminescence and Excitation Spectroscopy of the 325 Å-thick, 10^{12} cm^{-2}–n_s 1383 sample, as explained in the text. The arrows indicate the assignment of the lines and not the results of the Hartree calculations.

the exciton is no more the fundamental level has been calculated to be around 10^{11} cm^{-2} [29], which corresponds to a criterion $n_s a_0^2 \sim 0.06$ [30] if one takes a 75 Å value for the exciton radius in finite barrier height QW's. Unfortunately, the lack of a specific calculation applying to our samples and the relative importance of defect-related inhomogeneous broadening of excitonic lines prevent us to perform a line-shape analysis which would give an accurate experimental determination of this critical density. Nevertheless, in the limit $n_s = 0$, the electron-hole correlation amounts to the exciton binding energy, which is now well known both experimentally and theoretically [31, 32] (about 8 meV in a 150 Å-thick QW). By comparison with the Hartree calculations, one obtains a check of the calculations and/or of the sample parameters.

It is possible to plot the energy of the luminescence as a function of n_s deduced from the Stokes shift measurements (Fig. 9). Comparison with the Hartree calculation gives, as discussed above, the measurement of the BGR due to many-body effects. Tentative comparisons with some theoretical results not determined in the same structure geometry provide a fair agreement, although slight discrepancies remain, even in absolute calculations performed for a similar one-side 150 Å-thick MDQW with a carrier density $n_s = 4 \times 10^{11}$ cm^{-2} [33].

5. Luminescence from excited subbands in large n_s MDQW's

This luminescence has already been observed in a priori symmetrical but actually asymmetrical large n_s and large L MDQW's [3, 34]. Our aim is to perform a study including the oscillator strength calculation in a peculiar sample. Figure 10 shows the photoluminescence spectrum (dashed line) and the excitation (full line) spectrum of a 325 Å-thick, 10^{12} cm^{-2} n_s, one-side MDQW. The photoluminescence of the MDQW is composed of a strong peak at 1519 meV and of a broad weak line at 1500 meV. The photoluminescence of the GaAs buffer (dotted line) is also shown. Here also, the carrier density has been measured by Shubnikov–de-Haas measurements under the same illumination conditions as optical experiments. In the darkness, the first excited subband is found to be empty. Note that the poor quality of SdH measurements prevents us to determine the population of the excited subband under illumination.

The most striking feature of optical spectra is the small Stokes shift (between 1 and 2 meV) occurring between the first excitation peak and the main luminescence peak, in spite of the high carrier density which involves an electronic Fermi energy in the 30 meV range. The Hartree calculation performed following the method of Section 2 shows that the first excited subband E_2 is located only 26 meV above E_1 ($\varepsilon_1 = 79$ meV for a 106 meV total potential energy difference across the 325 Å-thick well). E_2 is already populated. For comparison with experiment, one needs a self-consistent calculation which takes into account the population of E_2. Nevertheless, as E_2 is marginally populated, the understanding of the main features is possible within our simple assumptions. For that purpose, the oscillator strengths of the optical transitions have been calculated at $k_\perp = 0$. Owing to a better overlap between the wavefunctions, the E_2–HH_1 transition is found 70 times more intense than the E_1–HH_1 one. The

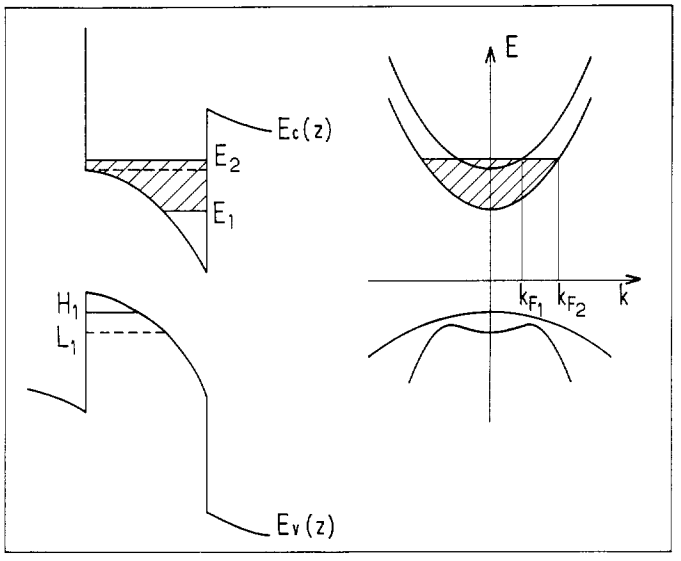

Fig. 11. Profiles of the conduction- and valence-band edges in the vicinity of a MDQW (left panel) and (right panel) schematic in-plane dispersion relations showing the two characteristic Fermi wave vectors when two conduction subands are populated.

Stokes shift between the first excitation peak and the main luminescence peak accounts approximately for the population of the excited subband, i.e., $(\varepsilon_F - \varepsilon_2)(1 + m_e/m_{hh})$ (Fig. 11). The energy difference between the first two peaks in excitation is well reproduced by the HH_1–LH_1 energy difference at $\boldsymbol{k}_\perp = (2m_e/\hbar^2)(\varepsilon_F - \varepsilon_2)$. The low energy line about 17 meV below the main luminescence peak can be assigned to the E_1–HH_2 transition. The bulk e–Å transition line near 1493 meV must overshadow the very weakly allowed E_1–HH_1 transition, if any.

It has not been possible to vary n_s in this sample by Argon illumination or by Schottky voltage application, perhaps due to the small spacer thickness and also to the proximity of the bulk luminescence. Nevertheless, and with the restriction that the Hartree calculation is only approximate, a 7 meV BGR value is found. Electrons are essentially located in a well whose shape is dictated by band bending, like in 150 Å-thick samples. Thus, the BGR for conduction states must be nearly the same as in the thinner wells. On the contrary, a decrease of the hole–electron correlation may be supposed. More detailed theories, both in the Hartree and Hartree–Fock schemes, are obviously required.

6. Conclusion

In conclusion, a detailed analysis of optical transitions in modulation-doped quantum-wells has been reported. With the use of a band gap renormalization, the data compare favorably with the results of self-consistent Hartree calculations of the energy levels which include a realistic description of the valence-band dispersion relations of the actual structures. The role of the first excited subband has been emphasized, when this level is populated. Moreover, a control of the electron density has provided a measurement of the density dependence of the band-gap renormalization due to many-body effects. The comparison with available theoretical models is fair although calculations taking into account the peculiar shape of the structures are required.

Acknowledgements

I would like to thank G. Weimann and W. Schlapp, from Forschungsinstitut der Deutschen Bundespost (Darmstadt), who have provided high-quality samples, and J. Orgonasi, M. H. Meynadier, J. A. Brum, G. Bastard and M. Voos for their contribution to this work. Discussions with J. C. Maan and complementary experiments in Hochfeld Magnetolabor des Max Planck Instituts für Feskörperforschung (Grenoble) were very useful. The Groupe de Physique des Solides is Unité Associée au Centre National de la Recherche Scientifique.

References

1. Abstreiter, G. and Ploog, K., Phys. Rev. Lett. **42**, 1308 (1979)
2. Inoue, K., Sakaki, H. and Yoshino, J., Jpn. J. Appl. Phys. **23**, L767 (1984).
3. Pinczuk, A., Shah, J., Miller, R. C., Gossard, A. C. and Wiegmann, W., Solid State Commun. **50**, 735 (1984).
4. Burkhard, H., Schlapp, W. and Weimann, G., Surf. Sci. **174**, 382 (1986)
5. Rice, T. M. in Solid State Physics (Edited by H. Ehrenreich, F. Seltz and D. Turnbull), Vol. 32, pp. 1–86, Academic, New York (1977).
6. Chemla, D. S., Schmitt-Rink, S. and Miller, D. A. B., To be published in Nonlinear Optical Properties of Semiconductors (Edited by H. Hang).
7. Tränkle, G., Leier, H., Forchel, A., Haug, H., Ell, C. and Weimann, G., Phys. Rev. Lett. **58**, 419 (1987).
8. Meynadier, M. H., Orgonasi, J., Delalande, C., Brum, J. A., Bastard, G., Voos, M., Weimann, G. and Schlapp, W., Phys. Rev. **B34**, 2482 (1986).
9. Delalande, C., Orgonasi, J., Meynadier, M. H., Brum, J. A., Bastard, G., Weimann, G. and Schlapp, W., Solid State Commun. **59**, 613 (1986).
10. Chaves, A. S., Penna, A. F. S., Worlock, J. M., Weimann, G. and Schlapp, W., Surf. Sci. **170**, 618 (1986).
11. Bastard, G., private communication.
12. Stern, F., Surf. Sci. **174**, 425 (1986).
13. Delalande, C., Brum, J. A., Orgonasi, J., Meynadier, M. H., Bastard, G., Maan, J. C., Weimann, G. and Schlapp, W., To appear in Superlattices and Microstructures.
14. Shah, J., Pinczuk, A., Störmer, H. L., Gossard, A. C. and Wiegmann, W., Appl. Phys. Lett. **44**, 322 (1984).
15. Deveaud, B., Emery, J. Y., Chomette, A., Lambert, B. and Baudet, M., Appl. Phys. Lett. **45**, 1078 (1985).
16. Meynadier, M. H., Delalande, C., Bastard, G., Voos, M., Alexandre, F. and Liévin, J. L., Phys. Rev. **B31**, 5539 (1985).
17. Bastard, G. Surf. Sci. **170**, 426 (1986).
18. Ando, T., J. Phys. Soc. Jpn. **51**, 3893 (1982).
19. Stern, F. and Das Sarma, S., Phys. Rev. **B30**, 840 (1984).
20. Altarelli, M. in Heterojunctions and Semiconductor Superlattices (Edited by G. Allan, G. Bastard, N. Boccara, M. Lannoo and M. Voos), Springer Verlag, Berlin (1986).
21. Ando, T. J. Phys. Soc. Jpn. **54**, 1528 (1985).
22. Ruckenstein, A. E., Schmitt-Rink, S. and Miller, R. C., Phys. Rev. Lett. **56**, 504 (1986).
23. Chemla, D. S. and Miller, D. A. B., J. Opt. Soc. Am. **B2**, 1155 (1985).
24. Schmitt-Rink, S., Chemla, D. S. and Miller, D. A. B., Phys. Rev. **B32**, 6601 (1985).
25. Kleinman, D. A. and Miller, R. C. Phys. Rev. **B32**, 2266 (1985).
26. Yia-Chung Chang and Sanders, G. D., Phys. Rev. **B32**, 5521 (1985).
27. Schmitt-Rink, S., Ell, C. and Haug, H., Phys. Rev. **B33**, 1183 (1986).
28. Bauer, G. and Ando, T., J. Phys. **C19**, 1537 (1986).
29. Kleinman, D. A., Phys. Rev. **B32**, 766 (1985).
30. Schmitt-Rink, S. and Ell, C., J. Luminesc. **30**, 585 (1986).
31. Greene, R. L., Bajaj, K. K. and Philips, D. E., Phys. Rev. **B29**, 1807 (1984).
32. Miller, R. C., Kleinman, D. A., Tsang, W. T. and Gossard, A. C., Phys. Rev. **B26**, 1974 (1982).
33. Bauer, G. and Ando, T., Phys. Rev. **B34**, 1300 (1986).
34. Meseguer, F., Maan, J. C. and Ploog, K. To be published in Superlattices and Microstructures.